

Vibrational Sum Frequency Spectroscopy on Pd(111) and Supported Pd Nanoparticles: CO Adsorption from Ultrahigh Vacuum to Atmospheric Pressure[†]

Holger Unterhalt, Günther Rupprechter,* and Hans-Joachim Freund

Chemical Physics Department, Fritz-Haber-Institut der Max-Planck-Gesellschaft, Faradayweg 4-6, D-14195 Berlin, Germany

Received: August 2, 2001; In Final Form: November 5, 2001

The adsorption of CO on Pd(111) and on Al₂O₃-supported Pd nanoparticles was studied by picosecond infrared–visible sum frequency generation (SFG) vibrational spectroscopy in a pressure range from 10⁻⁷ to 1000 mbar and in a temperature range of 100–520 K. Under ultrahigh vacuum (UHV), the samples were further characterized by low-energy electron diffraction (LEED), Auger electron spectroscopy (AES), and temperature-programmed desorption (TPD). Identical high coverage (saturation) CO structures were observed on Pd(111) under UHV conditions (10⁻⁷ mbar, 100 K) and at high pressure (e.g., 1 mbar, 190 K). No indications of pressure-induced surface rearrangements of Pd(111) were evident from SFG and LEED. SFG spectra of CO adsorption on “defect-rich” Pd(111) revealed an additional peak that was attributed to adsorption on defect (step or edge) sites. The CO adsorbate structure on supported Pd nanoparticles was found to be different from that on Pd(111) and to be more similar to that on stepped or strongly sputtered Pd(111). At low pressure, the adsorption site occupancy depended on the particle surface structure and temperature. CO preferentially adsorbed in bridge sites on well-faceted Pd particles, while on more defective Pd particles, on-top sites were occupied as well. However, at 200 mbar CO, an adsorption site occupancy was obtained that was nearly independent of the particle surface structure. While the surface structure of the Pd particles remained unchanged upon high-pressure gas exposure, an annealing treatment to 300–400 K was able to order the Pd particle surface. Gas mixtures of CO and hydrogen on Pd(111) showed SFG spectra similar to the pure CO case indicating the absence of a strong interaction between CO and hydrogen.

1. Introduction

Vibrational sum frequency generation (SFG) spectroscopy is a versatile interface-specific technique, which has been successfully employed to study a variety of solid–gas and solid–liquid interfaces.^{1,2} Its inherent sensitivity to media without inversion symmetry allows the monitoring of adsorbed species at the interface between centrosymmetric or isotropic phases, even in the presence of a gas phase or of a solvent. The advantages of SFG spectroscopy have been outlined in a number of previous publications covering a wide range of substrate (interface)–adsorbate combinations.^{1–6} The first applications of SFG to catalysis research were reported in the 1990s by groups in Annandale (Exxon),³ Berkeley⁷ and Jülich.⁸ In these studies, single-crystal surfaces such as Ni(100), Pt(111), and Pt(110) were utilized, but the field was soon extended to thin oxide films⁹ and polycrystalline foil.¹⁰ Recently, SFG spectra of CO on ultrahigh vacuum (UHV)-grown sub-10-nm Pd nanoparticles were obtained in our laboratory,¹¹ and CO adsorption on lithographically fabricated Pt aggregates (20–200 nm mean size) has been reported by Baldelli et al.¹² Because SFG spectroscopy can be applied both to single crystal surfaces and to supported nanoparticles and, in addition, can cover the pressure range from UHV to atmospheric pressure, it is clear that SFG is a key element to link surface science with “real” catalysis.

One of the long-standing questions is the relevance of surface science studies to catalysis, even when the simplest elementary

step, adsorption, is considered. Are adsorbate structures that are observed under typical UHV conditions (i.e., exposures of several langmuirs at 100–200 K) at all representative of adsorbate structures that are present under reaction conditions? How good are extrapolations over 10 or more orders of magnitude in pressure? If active species are weakly bound, they may only appear at high pressure after all of the strongly adsorbing sites on the surface are occupied, but they may be missed in UHV studies.⁶ The equilibrium with the gas phase and the elevated temperature may lead to adsorbate structures that cannot be observed under UHV. Furthermore, the high pressures, high temperatures, or both during a catalytic reaction may restructure the catalyst surface,^{13–16} which, in turn, would have an impact on the adsorbate structure. Such high-pressure surface rearrangements and adsorbate structures not appearing under UHV have in fact been observed for CO on Pt single-crystal surfaces.^{13,17}

Supported nanoparticles are certainly even more prone to faceting or sintering under reaction conditions. Therefore, it is clear that high-pressure studies should ideally be carried out on single crystals *and* nanoparticles, to also identify effects that are inherent to supported nanoparticles (e.g., their size-dependent geometric and electronic structure,¹⁸ support effects such as spillover, phase boundary sites, etc.¹⁶). A model system that mimics the complex properties of a supported catalyst but, most importantly, is still accessible to many surface analytical techniques (including SFG) will be described in section 2.2.

CO on Pd(111) was studied in UHV by a number of groups, for example, by the groups of Bradshaw,^{19,20} Hoffmann,²¹ Ertl,^{22,23} Somorjai,²⁴ Goodman,²⁵ Bourguignon,²⁶ and others,^{27,28} often using a combination of low-energy electron diffraction

[†] Dedicated to Prof. Friedrich Dörr on the occasion of his 80th birthday.

* To whom correspondence should be addressed. E-mail: rupprechter@fhi-berlin.mpg.de. Fax: +49 30 8413 4105.

(LEED), infrared reflection absorption spectroscopy (IRAS), and temperature-programmed desorption (TPD). IRAS spectra up to 10 mbar CO were reported by Goodman and co-workers^{25,29,30} allowing construction of a “phase diagram” of equilibrium CO structures. Pd nanoparticles on different oxide supports were examined by several groups.^{30–33}

In this paper, we present SFG vibrational spectra of carbon monoxide adsorbed on Pd(111), on “defect-rich” Pd(111), and on alumina-supported Pd nanoparticles at temperatures from 100 to 520 K and at pressures between 10^{-7} and 1000 mbar. The experiments, carried out in a UHV surface analysis system combined with an SFG-compatible UHV/high-pressure cell, revealed that the high-pressure CO spectra were comparable to those acquired under UHV conditions. No indications for high-pressure CO structures were found, but distinct differences were observed between the high-pressure CO adsorption on Pd nanoparticles and Pd(111). The reversibility of the UHV SFG spectra after high-pressure treatment indicated that permanent pressure-induced structural rearrangements were absent under our experimental conditions. However, annealing of rough nanoparticles resulted in the formation of ordered surface facets. Co-adsorption studies of CO and H₂ at elevated pressure up to 523 K indicated that CO adsorption is unaffected by the presence of hydrogen.

2. Experimental Section

2.1. Vibrational Sum Frequency Generation Spectroscopy (SFG). Vibrational sum frequency generation spectroscopy makes use of the second-order nonlinear optical process of sum frequency generation (SFG). In SFG, two light waves at different frequencies interact in a medium characterized by a nonlinear susceptibility tensor, $\chi^{(2)}$, and generate a wave at the sum of their frequencies. Because SFG is not allowed in media with inversion symmetry ($\chi^{(2)} = 0$ in the electric dipole approximation), the process can sensitively probe regions of broken inversion symmetry in otherwise centrosymmetric media, for example, the boundary between an isotropic gas phase and a centrosymmetric crystal. In the present case, the SFG signal is predominantly generated by adsorbed CO, while the centrosymmetric bulk of the Pd crystal and the isotropic gas phase give only a small contribution to the signal (see below). Because this nonlinear process generally produces only a small signal, high incident-light intensities, that is, pulsed lasers, are required.

In its spectroscopic application described here,³⁴ SFG allows the acquisition of vibrational spectra of adsorbates from submonolayer quantities in UHV up to ambient gas pressure. Because SFG uses photons to probe adsorbate vibrations, the requirement of a vacuum environment that limits electron spectroscopies (e.g., high-resolution electron energy-loss spectroscopy (HREELS)) does not apply. The basic principles of SFG spectroscopy and SFG spectrometers based on various lasers have been presented several times.^{1,3,4,6,9,11,35–38} Briefly, to acquire an SFG vibrational spectrum of adsorbate molecules on a catalyst surface, laser pulses at a tunable infrared frequency, ω_{IR} , and at a fixed visible frequency, ω_{vis} , are spatially and temporally overlapped on the sample. When the IR frequency is scanned over a vibrational resonance of the adsorbate, an SFG signal is generated at the sum frequency ($\omega_{\text{SFG}} = \omega_{\text{IR}} + \omega_{\text{vis}}$), that is, in the visible region. Plotting the SFG intensity as a function of the IR frequency (wavenumber) thus results in the vibrational spectrum.

The SFG signal is proportional to the absolute square of the (nonlinear) second-order surface susceptibility, $\chi_s^{(2)}$, and to the intensities, I_{IR} and I_{vis} , of the incident IR and vis pulses (eq 1).

It is therefore apparent that in the experiment the SFG signal must be normalized to the IR and vis intensities (which is particularly important in the presence of a gas phase, see below).

$$I_{\text{SFG}} \propto |\chi_s^{(2)}|^2 I_{\text{IR}} I_{\text{vis}} \quad (1)$$

$\chi_s^{(2)}$ has resonant contributions from the adsorbate vibrations, $\chi_{\text{R}}^{(2)}$, (containing the resonance condition ($\omega_{\text{IR}} - \omega_q$) and a nonresonant contribution from the surface itself, $\chi_{\text{NR}}^{(2)}$. In many cases, the applied light frequencies are far from resonances of the surface; its response is therefore usually modeled by a frequency-independent nonresonant susceptibility, $\chi_{\text{NR}}^{(2)}$ (assuming that this also contains the nonresonant contribution from higher-order multipole moments of the centrosymmetric bulk). Consequently,

$$\chi_s^{(2)} = \chi_{\text{R}}^{(2)} + \chi_{\text{NR}}^{(2)} = \sum_q \frac{A_{\text{R}(q)}}{\omega_{\text{IR}} - \omega_q + i\Gamma_q} + A_{\text{NR}} e^{i\Phi} \quad (2)$$

$$A_{\text{R}(q)} \propto NT_g M_g \delta\rho \quad (3)$$

where $\chi_{\text{R}}^{(2)}$, $\chi_{\text{NR}}^{(2)}$, $A_{\text{R}(q)}$, ω_q , Γ_q , and ω_{IR} refer to the resonant nonlinear susceptibility, nonresonant nonlinear susceptibility, amplitude, resonance frequency, and damping constant (homogeneous line width $2\Gamma_q = \text{fwhm}$) of the q th vibrationally resonant mode and to the infrared laser frequency, respectively. A_{NR} is the amplitude of the vibrationally nonresonant susceptibility, and Φ is its phase relative to the resonant term. The amplitude of the vibrationally resonant susceptibility, $A_{\text{R}(q)}$, is proportional to the adsorbate concentration (number density, N) and to the infrared and Raman transition moments of the vibration (T_g , M_g ; $\delta\rho$ is the population difference between the vibrational ground and excited state).

Considering the resonant term in eqs 2 and 3, it should be noted that the SFG intensity depends on the square of the adsorbate concentration but also on the infrared and Raman transition moments. Therefore, to be SFG active, a vibration must have nonvanishing infrared and Raman transition moments. Because these two terms might be different for different adsorbate geometries (e.g., bridge vs linear-bonded CO), the SFG signal cannot be easily correlated with the adsorbate concentration. A further complication may arise from the nonresonant background. Depending on its amplitude and phase difference, Φ , to the resonant term, the nonresonant susceptibility may cause strongly asymmetric line shapes. However, the resonant SFG signal is often much higher than the nonresonant background, producing almost Lorentzian-like line shapes in the spectra. In the experiments described here, the nonresonant background was small with a phase leading to rather symmetric SFG peaks. A semiquantitative analysis of the SFG spectra will be presented in a forthcoming publication.³⁹

2.2. Laser Setup and SFG-Compatible UHV–High-Pressure Cell. The SFG experiments on Pd(111) were performed using a Nd:YAG-based picosecond laser system (1064 nm, 30 mJ/pulse, 20 ps, 50 Hz). Part of the output was converted to 532 and 355 nm by a harmonic generator (SHG, THG) unit. About 200 $\mu\text{J}/\text{pulse}$ 532 nm light was utilized as the visible beam in the SFG experiment, the 1064 and 355 nm beams were mixed in an optical parametric generator/amplifier (OPG/OPA) to generate tunable infrared light (3–6 μm , ca. 200 $\mu\text{J}/\text{pulse}$, resolution $\sim 5 \text{ cm}^{-1}$) in a difference frequency generation (DFG) stage.

As illustrated by eq 1, the SFG intensity should depend linearly on the IR and vis intensities. Therefore, the SFG process

is not fully independent of the gas environment because at CO pressures above 1 mbar a significant part of the IR light is absorbed by the gas phase⁴⁰ (but no SFG signal is generated by gas-phase CO). To account for this effect, the IR energy reflected from the sample was measured during the SFG experiment, recalculated to the sample position (accounting for the additional absorption between the sample position and the IR detector) and used to normalize the SFG signal. Simultaneously, the vis intensity was recorded with a photodiode. In addition, small portions of the vis and IR beams were split and directed to a GaAs reference crystal to provide another control parameter. The SFG spectra were then normalized by dividing the experimental plots by the corresponding gas-phase absorption curves (for details, see ref 40). To prevent the attenuation of the IR beam by atmospheric CO₂ and water before entering the chamber, most of the beam path was encapsulated and purged with dry nitrogen.

SFG spectra of CO on Pd nanoparticles were acquired with another laser system based on an amplified titanium sapphire laser. About 90% of the output radiation (790 nm, 2 mJ/pulse, 2 ps, 500 Hz) was used to generate tunable infrared light (3–6 μm , ca. 10 μJ /pulse) with an OPG/OPA/DFG (resolution $\sim 25\text{ cm}^{-1}$). The infrared power was nearly constant between 2000 and 3300 cm^{-1} , but decreased below 2000 cm^{-1} because of a reduction of the transmission of the DFG AgGaS₂ crystal. Because the small IR energy could not be monitored directly during the experiment, GaAs reference spectra were acquired at varying CO pressures to normalize for IR absorption (GaAs produces a strong bulk SFG signal⁴⁰).

On both laser systems, the experiments were carried out using parallel-polarized IR and vis beams with 55° and 50° to the surface normal, respectively.^{40,41} This difference in the incident angles is necessary to separate the SFG signal from the pump beams by an aperture. The SFG signal is further filtered using an edge filter and a monochromator before it reaches a photomultiplier the signal of which is directed to a boxcar integrator and sent to a PC via an A/D interface. The IR frequency was calibrated to an accuracy of $\pm 3\text{ cm}^{-1}$ by measurements of the absorption bands of CO at high pressure and of atmospheric CO₂.

The combination of a surface analysis chamber with an SFG-compatible UHV–high-pressure cell allows us to prepare and characterize samples in UHV and to perform SFG experiments from 10^{-7} mbar to atmospheric pressure. Details of the two-level design were published elsewhere.⁴¹ Briefly, the upper level is an UHV system (base pressure, 1×10^{-10} mbar) equipped with low-energy electron diffraction (LEED), Auger electron spectroscopy (AES), and temperature-programmed desorption (TPD). The sample crystal is spot-welded to two Mo rods and can be resistively heated to 1300 K and cooled with liquid N₂ to 85 K (type K thermocouple). Using an *xyz* ϕ manipulator, the sample can be transferred under UHV to the SFG-compatible reaction cell in the lower level. When the manipulator is lowered to the SFG level, the sample holder is inserted into an arrangement of three differentially pumped spring-loaded Teflon seals and the SFG cell is separated from the UHV part. The SFG cell is pumped by its own turbomolecular pump, and the UHV environment is maintained during this operation. The SFG cell is equipped with two CaF₂ windows to allow infrared and visible light to enter and to allow sum frequency light to exit to the detector. When CO was introduced, the reaction cell could be pressurized up to 1 bar, while the upper chamber could still be kept at 5×10^{-10} mbar. To remove Ni- and Fe-carbonyl impurities, CO was passed over a carbonyl absorber cartridge

and then introduced via a cold trap filled with a liquid nitrogen/ethanol mixture (ca. 170 K). It should be noted that impurities in the $10^{-4}\%$ range (present in high purity CO) can be generally neglected under UHV conditions but have a significant partial pressure at high CO pressure (see below). To apply low exposures in UHV experiments, a leak valve and an ionization gauge were also connected to the SFG cell.

2.3. Preparation of Pd Surfaces. The Pd(111) single-crystal surface was prepared by standard cutting and polishing techniques and cleaned by a sequence of flash annealing to 1250 K, Ar ion bombardment (beam energy 700 eV at 2×10^{-4} mbar Ar at 300 K), annealing to 1200 K, oxidation in 5×10^{-7} mbar O₂ between 1200 and 600 K, and a final flash to 1200 K. The surface structure and cleanliness were examined by LEED, AES, and TPD (the TPD spectra were in agreement with data in the literature²⁷ and will be presented elsewhere³⁹).

“Defect-rich” Pd(111) surfaces, that is, slightly misoriented Pd(111) or strongly sputtered surfaces (700 eV Ar at 100 K, without subsequent annealing), were also studied. AES indicated that these surfaces were clean, but LEED showed a (1×1) pattern with rather broad spots.

Alumina-supported Pd nanoparticles were prepared according to a procedure that is described in detail in refs 42 and 43. An ordered aluminum oxide film was grown on NiAl(110) by oxidation in 10^{-5} mbar oxygen at 523 K. Pd was subsequently deposited on alumina using an electron beam evaporation source. By controlling the substrate temperature and the amount of metal, the cluster size and number density can be adjusted. Two different catalysts were prepared: Pd particles of 3.5 nm mean size (or 850 atoms per particle) grown at 90 K by depositing 0.6 nm Pd (particle density $4.5 \times 10^{12}/\text{cm}^2$) and Pd particles with 6 nm mean size (or 4000 atoms per particle) grown by depositing the same Pd amount at 300 K (particle density $1 \times 10^{12}/\text{cm}^2$).

Spot profile analysis–low energy electron diffraction (SPA–LEED)⁴² and atomically resolved scanning tunneling microscopy (STM) images of individual particles by Hansen et al.⁴⁴ have shown that the shape of Pd particles grown at 300 K closely resembles a truncated cuboctahedron (being one of the expected equilibrium shapes for a supported fcc metal particle⁴⁵). The particles grow with a (111) facet parallel to the alumina substrate and mainly expose a (111) top facet to the gas phase (and to a much smaller extent (111) and (100) side facets; Figure 1e). Figure 1c shows an STM image of Pd particles grown at 300 K.^{46,47} It should be noted that due to the “convolution” between the STM tip and the particle shape⁴² the Pd particles are imaged about twice as large and much closer to each other. However, the correct particle size can be calculated from the number density and the amount of evaporated metal and also by SPA–LEED.⁴²

If Pd is deposited at 90 K, the reduced mobility leads to a higher nucleation density and to a smaller particle size.⁴² No indication for well-developed facets has been found under these conditions, and we expect a less-ordered particle surface with more low-coordination sites (surface defects, edges, steps, etc.) due to the growth at lower temperature. Figure 1d shows a transmission electron micrograph (TEM) of Pd particles grown under the same conditions on a thin carbon film (supported by a copper TEM grid). The particle density ($4 \times 10^{12}/\text{cm}^2$) is very similar to that obtained on the Al₂O₃/NiAl(110) substrate, and the TEM image therefore provides a good representation of the particle size ($\sim 4\text{ nm}$) and the interparticle distance (in STM images the Pd particles seem to touch each other due to the tip effect). The higher resolution inset in Figure 1d shows a Pd

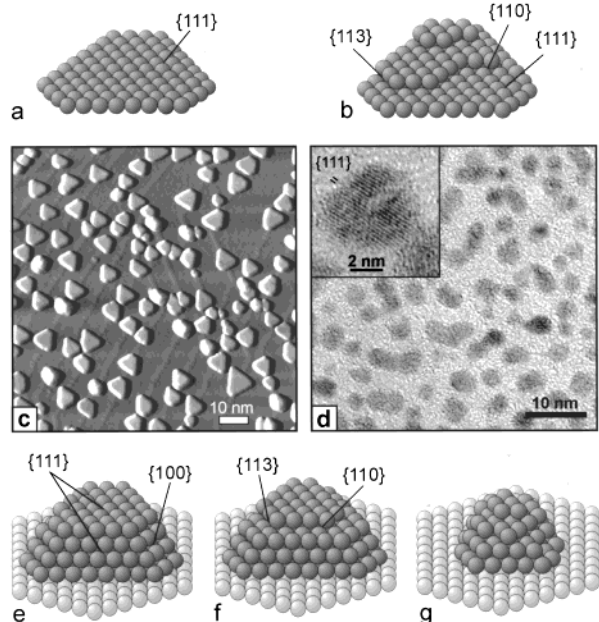


Figure 1. Schematic models of the different Pd surfaces employed in this study. A well-ordered Pd(111) and a “defect-rich” Pd(111) including various defects are shown in panels a and b. An STM image (CCT, 100 nm × 100 nm, adapted from refs 46 and 47) of Pd nanoparticles grown on Al₂O₃/NiAl(110) and a transmission electron micrograph are displayed in panels c and d; see text. Depending on the growth conditions, the Pd particles may have different morphologies and surface structures, for example, a well-faceted truncated cuboctahedron (panel e), with surface steps (panel f), and highly defective (panel g).

particle with {111} lattice fringes thus proving the crystalline nature of the particles. An extensive TEM investigation of Pd particles grown on Al₂O₃/NiAl(110) has been presented in refs 48 and 49.

Figure 1 shows schematic models of the different Pd surfaces together with an STM image and a TEM micrograph of Pd nanocrystals. The structural characteristics will be discussed in the following.

3. Results and Discussion

3.1. Adsorption of CO on Pd(111) from 10⁻⁷ to 1000 mbar.

CO on Pd(111) is one of the prototypical and most extensively studied systems in surface science. Vibrational spectroscopy, for example, by IRAS or HREELS, is a powerful technique to study the interaction of CO with well-ordered single-crystal surfaces, and in many cases, the observed CO stretching frequency allows identification of specific binding sites (terminal, 2-fold bridging, 3- and 4-fold hollow²¹). For CO on Pt, an empirical relation has been suggested that correlates the frequency of terminal CO with the coordination number of the binding Pt atom⁵⁰ (hence allowing distinction of terrace, step, and kink sites). It should however be kept in mind that binding site assignments that are solely based on vibrational frequencies may be incorrect, as shown, for example, by photoelectron diffraction.⁵¹ The coupling between CO molecules on different sites (e.g., CO on a terrace and a step edge) may lead to a resonance frequency that is different from the singleton frequencies of the individual sites. Therefore, a particular resonance frequency may not be characteristic for a specific (geometric) site but may be the result of the coupling between nearby vibrational modes (for details, see Greenler et al.^{52,53}).

CO on Pd(111) has been repeatedly studied by IRAS, LEED, and TPD, for example, by the groups of Bradshaw,^{19,20}

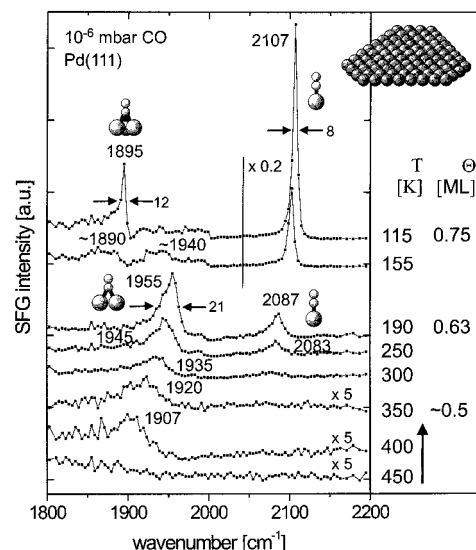


Figure 2. SFG spectra of 10⁻⁶ mbar CO on Pd(111) from 450 to 115 K. The spectra were recorded from high to low temperature. Coverages as determined from TPD are also indicated.³⁹

Hoffmann,²¹ Ertl,^{22,23} Somorjai,²⁴ Goodman,²⁵ and others.²⁷ As shown by Doyen and Ertl,⁵⁴ the close-packed (111) surface is energetically “smooth” for CO adsorption and the low surface diffusion barriers facilitate ordering of the adsorbate layer. Accordingly, a variety of ordered CO structures has been determined with a ($\sqrt{3} \times \sqrt{3}$)R30° at 0.33 ML, a c(4 × 2) at 0.5 ML, a (4 $\sqrt{3}$ × 8)rect at 0.63 ML, and a (2 × 2) at 0.75 ML as the most prominent structures (1 ML equals the density of Pd atoms in the (111) plane; 1.53 × 10¹⁵ cm⁻²). The vibrational spectrum of CO on Pd(111) strongly depends on coverage, and it is more complex than that of CO on Pt(111).⁴⁰

According to an IRAS study by Tüshaus et al.,¹⁹ CO initially adsorbs in 3-fold hollow sites with stretching frequencies from 1830 to 1900 cm⁻¹. At half monolayer coverage, a peak at 1920 cm⁻¹ was reported and originally attributed to bridge-bonded CO. However, recent photoemission and photoelectron diffraction studies^{28,55} and stretching frequency calculations⁵⁶ have shown that CO occupies fcc and hcp 3-fold hollow sites at $\theta = 0.5$. Around $\theta = 0.6$ –0.7, CO is preferentially bridge-bonded (~1960 cm⁻¹) with a smaller amount of linear (on-top) CO (~2090 cm⁻¹). If the coverage is further increased, the bridge-site intensity decreases, and finally, at saturation coverage (2 × 2, $\theta = 0.75$), two intense bands at 1895 and 2110 cm⁻¹ (hollow and on-top CO) are observed.

Figure 2 shows a series of SFG spectra of Pd(111) exposed to 10⁻⁶ mbar CO acquired at decreasing temperature from 450 to 115 K. CO coverages as determined by TPD (and by comparison with previous LEED/TPD studies^{19,22,23,25,27,39}) are also indicated. Adding CO at high temperature and cooling afterward generally produced better-ordered structures and avoided less-ordered nonequilibrium adsorption configurations.^{25,26,30,39} Some selected LEED images are presented in Figure 3.²² The series in Figure 2 is comparable to an isothermal exposure series in UHV except that here the coverage is increased by decreasing the substrate temperature. At 400 to 350 K, a small SFG signal at 1910–1920 cm⁻¹ was observed that had previously been attributed to bridge- or hollow-bonded CO at half monolayer coverage. With decreasing temperature, that is, increasing coverage, the peak shifted to higher wavenumber and a second peak characteristic of the stretching vibration of terminal (on-top) CO evolved. At 190 K, the spectrum consisted of two distinct peaks at 1955 cm⁻¹ (bridge-

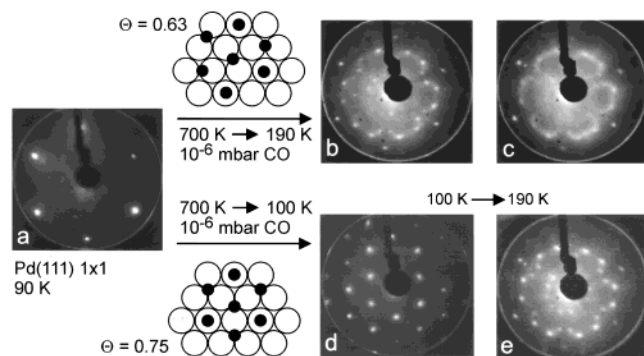


Figure 3. LEED images of CO structures on Pd(111): (a) the clean (1 × 1) Pd(111) surface; (b) after cooling the surface in 10⁻⁶ mbar CO from 700 to 190 K producing a surface coverage of 0.63 ML. This structure is sensitive to the electron beam and converts to the structure in panel c within a few seconds. A (2 × 2) structure with 0.75 ML coverage is obtained after cooling the surface in 10⁻⁶ mbar CO from 700 to 100 K. The corresponding structural models, adapted from Tüshaus et al.,¹⁹ are also shown (small circles, CO; big circles, Pd).

bonded CO) and 2087 cm⁻¹ (on-top CO) at a coverage of 0.63 ML (in good agreement with an SFG study by Bourguignon et al.²⁶). This structure exhibits the characteristic “flower” LEED pattern shown in Figure 3b,c. When the temperature was further decreased, the bridge peak shifted back to lower wavenumber and disappeared while the on-top peak grew and shifted to higher frequency. At 115 K, saturation (0.75 ML) was obtained and the LEED image of Figure 3d was observed. The corresponding SFG spectrum exhibits two peaks characteristic of hollow CO (1895 cm⁻¹) and of on-top CO (2107 cm⁻¹).^{19,25} Structural models by Bradshaw, Hoffmann, and others,^{20–22} based on LEED and IRAS data, are also shown in Figure 3 (for refined models, see refs 19 and 55).

The SFG spectra in Figure 2 qualitatively reproduce IRAS data obtained under UHV conditions. However, differences can be recognized that are most likely due to the different selection rules of SFG and IRAS. When Figure 2 is compared with corresponding spectra in refs 19, 21, and 25, it is evident that SFG “underestimates” multiple-coordinated CO thus leading to a dominant on-top peak. In particular, the hollow peak at 1895 cm⁻¹ is too small and the same is probably true for bridge-bonded CO (a similar effect occurs for CO/Pt(111)^{8,40,57}). Because the SFG intensity depends on both the infrared and Raman transition moments (besides, of course, the adsorbate surface concentration), the low sensitivity of SFG toward multiple-coordinated CO had been attributed to its low Raman polarizability. For this reason, a quantitative coverage analysis from the peak heights is difficult. However, the strong coverage dependence of the CO stretching frequency allows us to monitor (or approximate) the surface coverage.

The line widths of the on-top and hollow peak at 0.75 ML (8 and 12 cm⁻¹) and of the bridge peak at 0.6 ML (21 cm⁻¹) are similar to values reported from IRAS (on-top, 9 cm⁻¹; hollow, 17 cm⁻¹; bridge, 14 cm⁻¹).²¹ The SFG bridge peak is broader, but this is not a temperature effect (we observed a similar peak position and width at 90 K³⁹). The peak widths were taken directly from the spectrum and should be considered an upper limit (a deconvolution with the OPG resolution was not performed).

A peak at 2158 cm⁻¹ that was attributed to linear CO at antiphase domain boundaries of the adsorbate^{25,26} was not observed in our study. The absence of this peak is due to our dosing procedure at elevated temperature, which produced better-ordered CO structures, in agreement with the observation

of Bourguignon et al.^{26,58} that after annealing to 330 K the 2158 cm⁻¹ sites disappeared and were not repopulated upon cooling.

Under UHV, high surface coverages can be obtained by increasing the exposure or by decreasing the crystal temperature, while at the elevated temperature of a catalytic reaction, high coverages are achieved by high pressure. It is tempting to test whether both ways produce similar high-coverage structures. Figure 4 shows a “pressure series” on Pd(111) at 190 K. The first SFG trace was taken from the clean surface and shows a small invariant nonresonant background (denoted “nr bg”). The spectrum at 10⁻⁶ mbar displays bridge and on-top CO, in agreement with the corresponding spectrum in Figure 2. With increasing pressure, the bridge species (1955 cm⁻¹) disappears, on-top CO (2087–2107 cm⁻¹) grows, and hollow CO (1895 cm⁻¹) evolves.

At 10⁻⁶ and 10⁻⁴ mbar, two on-top species can be observed. The 2087 cm⁻¹ resonance is replaced by the 2099 cm⁻¹ peak upon increasing the pressure, and finally an on-top frequency of 2107 cm⁻¹ is obtained (see also Figure 9b). An apparent explanation would be to assign the 2087 cm⁻¹ peak to CO linearly bound to steps or defects and to assign the 2099 cm⁻¹ peak to on-top CO on the (111) terraces. If we assume that the defect concentration is very low, the different on-top frequencies may originate from dipole-coupling (and not from different on-top sites). In that case, the coexistence of two on-top species would indicate that two CO domains with slightly different coverage were present (isotope experiments would help to answer this question). The bridge peak is probably too broad to show such a splitting.

The “phase transition” from the bridge/on-top (0.63 ML) to the hollow/on-top (0.75 ML) structure²⁵ occurs between 10⁻³ and 1 mbar. Between 1 and 500 mbar, the on-top peak grows slightly but otherwise the spectra are identical. The reason for the decrease of the on-top signal above 500 mbar is probably related to the IR normalization. A real disappearance of on-top CO is unlikely because the on-top peak, which is located at an IR absorption maximum (see ref 40), decreased without a frequency shift while the hollow peak, which is outside the IR absorption range, remained constant. Above 500 mbar CO, the absorption of the IR light is very strong and a small error in the measurement of the low-intensity reflected IR may lead to incorrect peak heights.

A comparison of Figures 2 and 4 shows that the high-pressure adsorbate structures of CO up to 1000 mbar at 190 K are very similar to the high-coverage structures observed under UHV conditions by SFG or IRAS. There is no evidence for the formation of high-pressure species that are different from those under UHV. While high CO pressures have been reported to disrupt Rh nanoparticles¹⁴ and restructure Pt single crystals,¹³ under our experimental conditions such an effect was absent for Pd(111). The spectra were fully reversible with pressure, and the 10⁻⁶ mbar spectrum could be reproduced with high accuracy even after several hours of gas exposure (Figure 5, compare also the 1 mbar spectrum in Figure 4). Small differences may be due to carbon deposition, which is probably unavoidable in light of the time scale of the experiment (one spectrum takes about 15 min). LEED images obtained after pumping out CO were identical to Figure 3b, and after heating to 700 K and cooling to 90 K, a (1 × 1) LEED pattern was observed. In summary, no evidence for major surface rearrangements has been found.

The spectrum at 10 mbar CO and 190 K in Figure 4 agrees well with the corresponding IRAS spectrum reported by Kuhn, Szanyi, and Goodman²⁵ (except for peak intensities). Goodman

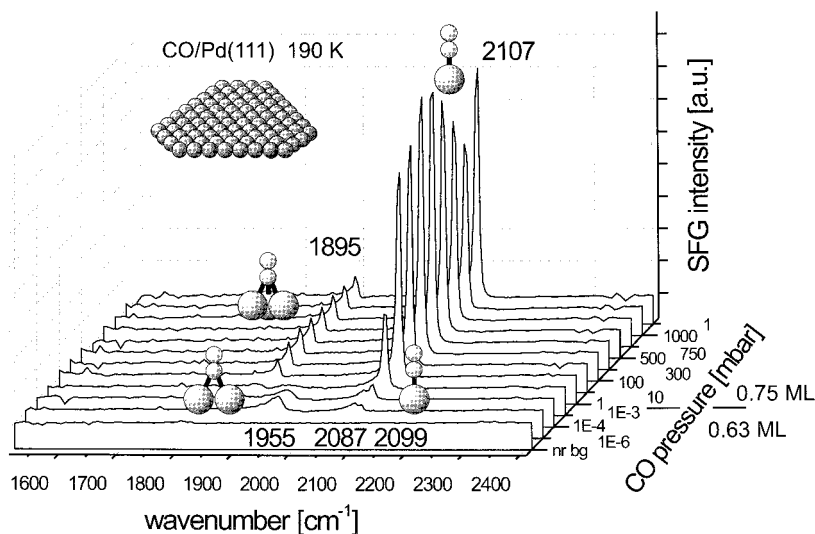


Figure 4. SFG spectra of CO adsorption on Pd(111) at 190 K from 10^{-6} to 1000 mbar. The final spectrum at 1 mbar demonstrates the reversibility of the adsorbate structure.

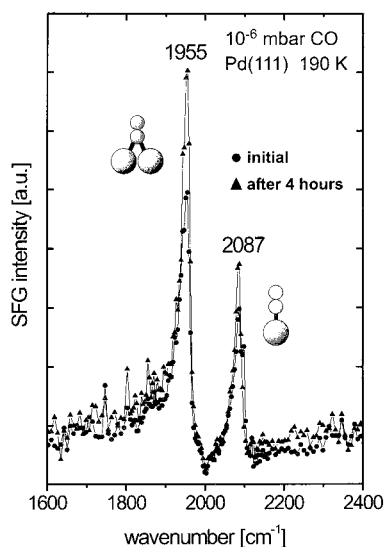


Figure 5. SFG spectra of 10^{-6} mbar CO on Pd(111) at 190 K: initial spectrum (●); after 4 h of high-pressure exposure (▲).

and co-workers have removed the gas-phase contribution by subtracting IR gas-phase spectra (measured on the clean Pd(111) surface around 1000 K) from the sample spectra. This allowed them to monitor the bridge/on-top to hollow/on-top transition up to 10 mbar and up to 1000 K. On the basis of these data, a phase diagram of the various CO structures was constructed.²⁵ At 190 K, a phase transition at 10^{-3} mbar was suggested, which is identical with our experimental result. Although Goodman and co-workers did not take spectra above 10 mbar CO, they have predicted phase-transition pressures for higher temperatures, for example, around 650 mbar CO for 300 K.

Figure 6 shows a pressure series that we have measured between 10^{-6} and 1000 mbar CO on Pd(111) at 300 K. At 10^{-6} mbar and 300 K, a coverage of about 0.5 ML was observed, in agreement with the corresponding spectrum in Figure 2. The coverage increased with increasing pressure and reached about 0.6 ML at 100 mbar. It should be noted that at 190 K this structure (coverage) was obtained already at 10^{-6} mbar. At ~ 0.6 ML, the line widths at 300 K were about 1.4 times bigger than those at 190 K. Upon further increasing the pressure, the bridge peak decreased and the on-top peak grew. Above about 700 mbar, a small hollow peak could be observed,

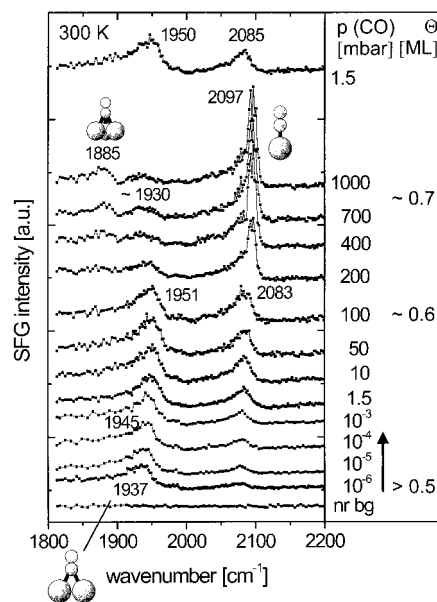


Figure 6. SFG spectra of CO adsorption on Pd(111) at 300 K from 10^{-6} to 1000 mbar. The final spectrum at 1.5 mbar demonstrates the reversibility of the adsorbate structure.

in fair agreement with the pressure predicted by Goodman and co-workers.²⁵ However, a perfect hollow/on-top structure could not be obtained under these conditions. The 1.5 mbar spectrum was repeated at the end of the series, and the reproducibility again indicates the absence of irreversible surface rearrangements or contamination. All surfaces were inspected by AES after the experiments, but no impurities (except small amounts of carbon) were detected.

In summary, the high-pressure CO spectra on Pd(111) were comparable to the high-coverage structures observed under UHV conditions. No evidence for high-pressure species or major surface restructuring was observed. In a previous paper on Pt(111),⁴⁰ we have stressed that great care has to be taken to control the CO cleanliness during high-pressure experiments. For Pt(111), we have observed that coadsorbed water induces a red shift of the on-top CO frequency. When long-time experiments are carried out below the desorption temperature of water (~ 160 K for Pt and ~ 175 K for Pd), water traces from the residual gas cannot be fully excluded. The effect of

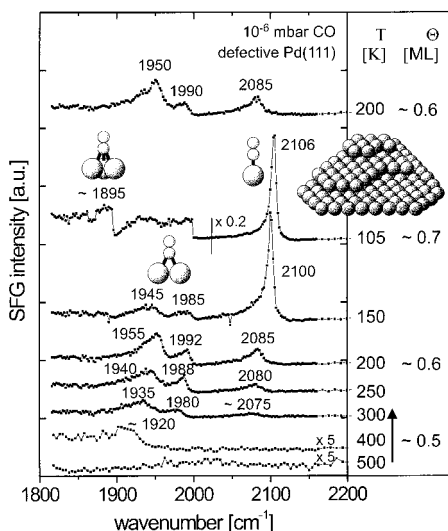


Figure 7. SFG spectra of 10^{-6} mbar CO on “defect-rich” Pd(111) from 500 to 105 K. The spectra were recorded from high to low temperature. Approximate coverages are also indicated.³⁹ When compared to the perfect (111) surface an additional peak at 1980–1990 cm^{-1} appeared.

coadsorbed water (which did not shift the CO frequency) will be treated in a separate article.³⁹ In the following, the results on Pd(111) will be compared to SFG spectra of CO adsorbed on “rough” Pd(111) and alumina-supported Pd nanoparticles.

3.2. Adsorption of CO on Defect-Rich Pd(111). The SFG spectra in Figure 7 were taken from a “defect-rich” Pd(111) surface, as described in section 2.3. AES indicated that the crystal was clean, but LEED showed a (1×1) pattern with broad spots. The crystal surface can be imagined as being composed of (111) terraces and all sorts of “defects”. These defects may include steps and kinks, and the steps can be also be regarded as (110) or (113) microfacets (or more precisely nanofacets). The temperature series in Figure 7 is very similar to the corresponding spectra of the well-ordered (111) surface (Figure 2) except that on the imperfect surface an additional peak is observed at 1980–1990 cm^{-1} . It is therefore apparent that this species is related to CO adsorbed on step (low-coordination) sites. The frequency range (1980–1990 cm^{-1}) suggests that it is a defect-related bridge-bonded species, for example, bridged CO on a step edge. Bridge-bonded species around 1985 cm^{-1} have also been assigned to CO on Pd(100),^{20,59,60} Pd(110),^{30,32,61} Pd(210),^{20,21} and rough Pd thin films.^{21,62}

The physical origin of the species at 1980–1990 cm^{-1} may be explained in several ways. It may originate from a specific binding site at a step edge (or nanofacet), but it may also arise from coupling between CO molecules on a step and neighboring CO molecules on a (111) terrace. Greenler and co-workers⁵⁰ have demonstrated that by dipole coupling of linear CO molecules on a step edge (where the metal atoms have coordination numbers of <9) and (subsequent) coupling to CO adsorbed on the terrace sites (coordination number = 9) a resonance frequency is produced that is characteristic rather for the ensemble and not so much for a particular binding site. In any case, this resonance frequency should be also found for CO adsorption on curved and rough surfaces of nanoparticles and has indeed been observed by infrared spectroscopy on Pd particles on silica prepared by impregnation,^{31,63} and on alumina-^{30,33} and titania-supported³² Pd model catalysts. It should be noted that the bridge/on-top to hollow/on-top transition again occurs around 1 mbar on the imperfect Pd(111) crystal at

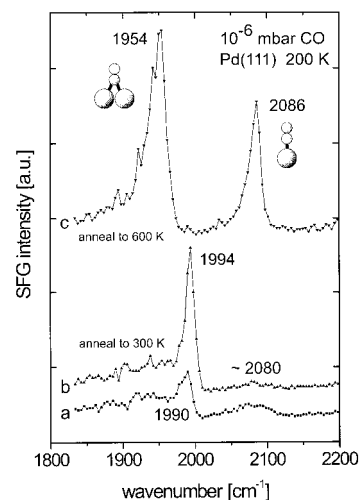


Figure 8. Effect of sputtering on the SFG spectra of CO on Pd(111) at 200 K: (a) 10^{-6} mbar CO on a strongly sputtered surface; (b) after annealing to 300 K. The observed peak is characteristic of a defect-related bridge site. After annealing to 600 K (c), a vibrational spectrum typical of perfect Pd(111) is obtained. All spectra were recorded at 200 K.

190 K (not shown), that is, it is nearly identical to Pd(111) and seems not to be heavily influenced by the presence of defects.

To deliberately introduce defects on a smooth Pd(111) surface, we sputtered the surface at low temperature (700 eV Ar^+ at 100 K) without subsequent annealing. Figure 8 shows a sequence of spectra acquired on such a sputtered surface. At 10^{-6} mbar CO and 200 K (Figure 8a), a bridge peak and a broad band in the on-top region were observed but the bridge peak had a resonance frequency characteristic for the defect/step sites (1990 cm^{-1}) described above. When the surface was heated to 300 K in the gas and cooled to 200 K again, the bridge species increased in intensity (Figure 8b). This ordering effect is also known from the regular (111) surface. When CO is exposed at higher temperature and the crystal is cooled, the higher mobility of CO allows it to obtain better-ordered structures. However, when the sample was annealed to 600 K and cooled, the regular bridge species at 1954 cm^{-1} and a sharp on-top peak were observed (Figure 8c). Obviously, on Pd(111), annealing to 600 K is sufficient to heal defects produced by sputtering.

3.3. Adsorption of CO on Pd/Al₂O₃ from 10^{-7} to 200 mbar. We will now compare the results described above to SFG spectra of CO on alumina-supported Pd nanoparticles.¹¹ Two aspects will be considered: the relative ratio of on-top/bridge adsorption and the resonance frequencies. Part of the SFG spectra were reported in previous publications.^{11,64} However, they were measured before the Pd(111) “reference” SFG spectra, and some of the observations were therefore not fully understood. These spectra will be discussed in this paper and completed with new results. The optical parametric generator/amplifier (OPG/OPA) utilized in the cluster experiments to generate the IR radiation had a resolution of only $\sim 25 \text{ cm}^{-1}$, and frequencies below 1900 cm^{-1} were not accessible because of the low IR energy in this range. Nevertheless, the cluster spectra can still provide valuable information on the CO adsorbate structure, as shown below.

Figure 9a shows SFG spectra of CO on Pd particles of 6 nm mean size (about 4000 atoms/particle) taken at 190 K between 10^{-7} and 200 mbar CO background pressure (at higher pressure the signal became very small because of IR absorption). The Pd particles were grown at 300 K and mainly exhibited (111) and (100) surface facets, as shown in Figure 1c,e.^{42,44,46,47} The

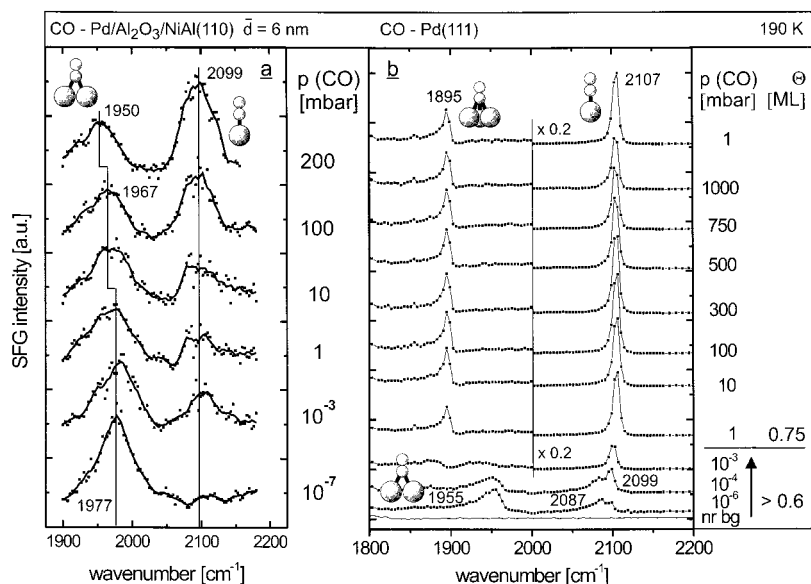


Figure 9. Comparison of CO adsorption on Al₂O₃-supported Pd nanoparticles (mean size 6 nm) and on Pd(111) at 190 K (see text).

(111) top facet dominates the particle morphology because the contribution of (111) and (100) side facets is rather small. In addition, CO adsorbed on the side facets is tilted with respect to the underlying metal substrate and, according to the IR surface-selection rule, should produce only a small signal.²¹ Therefore, the 6 nm particles should behave similarly to a (111) surface, and the corresponding single-crystal spectra are shown in Figure 9b (for ease of comparison the spectrum of Figure 4 was re-plotted in a different way). The 10⁻⁷ mbar CO spectrum on the Pd particles is indeed similar to the 10⁻⁶ mbar spectrum on Pd(111). In both cases, CO preferred to bond as a bridging species and only a small on-top peak was observed. It was mentioned before that a quantitative analysis is difficult, but if we take the integrated SFG signal intensity as a rough estimate, the on-top/bridge ratio is ~0.2 on Pd(111) and <0.1 on the nanoparticles. However, the frequency of the bridge species is different. The bridge peak on the nanoparticles (1977 cm⁻¹) is characteristic for defective (stepped) Pd(111) rather than CO bridge bonded to a perfect (111) terrace (1955 cm⁻¹).

Several explanations may account for this observation. The ball model in Figure 1e is certainly an idealized model (for a given size, a truncated cuboctahedron with complete surfaces would consist of a “magic number” of atoms). During the particle growth by vapor deposition, the number of Pd atoms per particle is continuously increased and consequently some surface steps must be present even on well-faceted nanoparticles. The particle will have monatomic steps, and such steps have been actually imaged by high-resolution transmission electron microscopy^{49,65} and STM (see Figure 5 (top) in ref 46). This is equivalent to the presence of {110} and {113} nanofacets. It is therefore not surprising that the resonance frequency of bridge-bonded CO is different on nanoparticles and on Pd(111). As discussed in section 3.2, the observed frequency is not necessarily characteristic for a specific binding site but may represent the whole ensemble. The coupling of CO molecules bound to steps and particle edges to those on the terraces may give rise to a peak that cannot be observed on the perfect Pd(111) surface. Density functional studies of CO adsorption on cuboctahedral Pd nanoparticles by Neyman and Röscher⁶⁶ have indeed shown that the vibrational frequency of bridge-bonded CO on the particle edges is different from that of bridge-bonded CO on the terraces.

IRAS spectra of Pd/Al₂O₃/NiAl(110) by Wolter et al.,³³ which provide higher spectral resolution, have identified two bridge-bonded species on large well-faceted Pd particles at saturation coverage of CO. The dominant species was defect (edge or step)-related bridge-bonded CO (around 1990 cm⁻¹), but a smaller peak due to CO bridge bonded to “perfect” (111) terraces at ~1950 cm⁻¹ (i.e., at the (111) single-crystal value) was also evident (these peaks are often termed B₁ and B₂ bands^{31,32,63}). A similar result was reported by Rainer et al.³⁰ for Pd/Al₂O₃/Ta(110) attributing the 1990 cm⁻¹ peak to (100) facets and by Yates and co-workers³¹ for Pd/SiO₂. In any case, the 1950 cm⁻¹ peak is probably too weak for our SFG setup.

When the CO pressure was increased, the bridge-bonded CO peak decreased in intensity and shifted to lower wavenumber while the on-top peak increased (on-top/bridge ratio at 10⁻³ mbar, 0.5; at 1 mbar, 0.5; at 10 mbar, 0.7; at 100 mbar, 1.2; at 200 mbar, 1.7). Similar spectral changes can be seen on Pd(111) in Figure 9b during the bridge/on-top to hollow/on-top transition. It seems that the CO coverage on the nanoparticles is increased but the 0.75 ML structure is not reached—the bridge peak had not even disappeared at 200 mbar. Gelin and Yates³¹ and Rainer et al.³⁰ report a similar behavior for Pd particles on silica and alumina. This effect is probably related to the heterogeneity of the particle surface that prevents the phase transition from (fully) occurring. If this argument—based on surface roughness—is true, then one would expect a different SFG spectrum on defect-rich “rough” Pd particles.

Figure 10 shows the corresponding SFG spectra of CO adsorbed on 3.5 nm Pd particles (about 850 atoms/particle) grown at 90 K. These particles exhibited “rough” surfaces with many defects and distinct facets were absent⁴² (Figure 1g). The bridge frequency was again found at 1978 cm⁻¹ indicating a defect-related bridge species. While on Pd(111) and on the 6 nm particles the on-top peak was rather small, a pronounced on-top peak was observed on the 3.5 nm nanoparticles (on-top/bridge ratio of ~1.1), in good agreement with impregnated samples.^{63,67} The higher abundance of on-top CO is a clear indication of the highly defective surface of the nanoparticles. On rough particles, many defect sites, for example, protruding Pd atoms, are available and lateral CO interactions are much reduced, and this presumably favors a higher fraction of on-top CO.

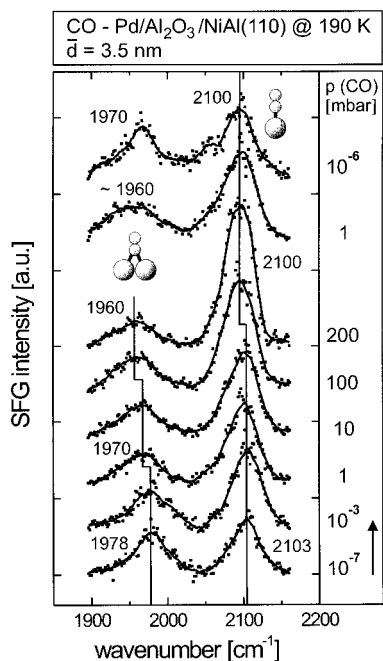


Figure 10. SFG spectra of CO adsorption on Al_2O_3 -supported Pd nanoparticles at 190 K and between 10^{-7} and 200 mbar. The Pd particles had a mean size of 3.5 nm and were expected to have rough surfaces due to their growth at 90 K. At low pressure, a higher fraction of on-top CO is observed on the “rough” Pd particles when compared to well-faceted nanocrystals (cf. Figure 9a).

If the SFG spectra of the 6 and 3.5 nm Pd particles at 10^{-7} mbar are compared, it is evident that the adsorption site occupancy is different. If this would be directly extrapolated to the high-pressure regime, one is tempted to explain any difference in the catalytic activity of the 6 and 3.5 nm Pd particles by the different adsorption site distribution. However, as discussed below, this assumption is incorrect.

Upon increasing the CO pressure on the 3.5 nm Pd particles (Figure 10), similar changes as for the 6 nm particles were observed (frequency shift and intensity decrease of bridge-bonded CO, intensity increase of on-top CO; on-top/bridge ratio at 10^{-7} mbar of 1.1; at 10^{-3} mbar of 1.6; at 1 mbar of 2.2; at 10 mbar of 2.2; at 100 mbar of 2.5; at 200 mbar of 4.4; at 1 mbar of 1.9; at 10^{-6} mbar of 1.4). At high pressure (e.g., 200 mbar), an adsorption site occupancy was achieved that is very similar for both particle sizes. The pressure series in Figure 10 again shows the tendency toward a bridge/on-top to hollow/on-top transition, but this process is still incomplete at 200 mbar because of the heterogeneity of the surface. In contrast, on smooth Pd(111), even a pressure of 1 mbar was enough for the disappearance of bridge-bonded CO (Figure 9b). The defect concentration on defect-rich Pd(111) was probably not high enough to prevent the phase transition (cf. Figure 7). When the pressure was decreased, the initial spectra could be reproduced indicating the absence of structural changes.

Similar spectra were also taken at 300 K (Figure 11). Because 300 K is already above the desorption temperature of on-top CO on Pd clusters, the adsorption behavior was drastically changed. Even for the 3.5 nm Pd particles (Figure 11b), only a small on-top peak could be observed by SFG at 10^{-7} mbar (this may be partly related to heating the particles grown at 90 K to 300 K; see below). With increasing pressure, the bridge species shifted to higher wavenumber and the on-top peak grew. However, at 300 K, the on-top peak never exceeded the bridge peak. The spectral behavior was similar to the 300 K series on Pd(111) (Figure 6). At low pressure, the bridge species had not

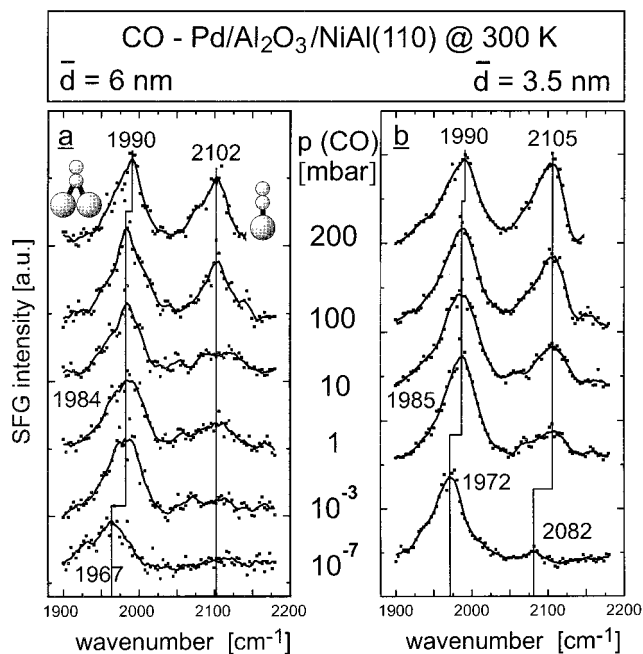


Figure 11. SFG spectra of CO adsorption on Al_2O_3 -supported Pd nanoparticles at 300 K and between 10^{-7} and 200 mbar. The Pd particles had a mean size of 6 (a) and 3.5 nm (b). On-top CO could be repopulated above 1 mbar.

reached its maximum coverage and the on-top peak was very small. The bridge peak was hence shifted to higher wavenumber with pressure, and the on-top peak started to develop. A coverage of 0.5–0.6 ML and an on-top CO ratio of about 0.6 were only obtained around 100 mbar CO (on-top/bridge ratio at 1 mbar, 0.4; at 10 mbar, 0.5; at 100 mbar, 0.6; at 200 mbar, 0.8). Of course, the bridge frequency on the nanoparticles was again related to the surface defects. A shift to lower wavenumbers would be expected if the CO pressure would be further increased, but it is unlikely that the phase transition would occur.

Finally, it should be mentioned that the 10^{-7} mbar particle spectra could be reproduced after the high gas pressure was pumped out (in agreement with the behavior of impregnated Pd/SiO₂ catalysts³¹). At temperatures up to 300 K, no indications for particle disruption upon CO exposure were observed. To test the possibility of laser-induced photodesorption or thermal desorption, a series of consecutive spectra at 10^{-7} mbar and 190 K was measured. Within our spectral sensitivity and accuracy, we did not detect any changes in the spectra (even after 3 h).

Figure 12 shows the effect of increasing temperature (annealing) on the adsorbate structure. The SFG spectra were taken at 10^{-7} mbar CO on 3.5 nm Pd particles grown at 90 K. At 115 K, a spectrum typical for “rough” Pd particles was observed, exhibiting peaks at 1990 and 2112 cm^{-1} . The spectrum at 190 K is very similar to the corresponding spectrum in Figure 10 with a bridge and an on-top peak of comparable intensity (on-top/bridge ratio of 0.8). With increasing temperature, the CO coverage was reduced and, in agreement with the single-crystal data (Figure 2), the on-top peak disappeared between 250 and 300 K. At the same time, the bridge peak was shifted to lower wavenumber and reached 1972 cm^{-1} at 300 K. When the temperature was lowered back to 190 K, the spectrum showed the same species as prior to the annealing treatment (1988 and 2110 cm^{-1}) but the on-top fraction was reduced to 0.2. After annealing to 300 K, the spectrum is now similar to a spectrum of well-faceted particles (grown at 300 K). After heating the

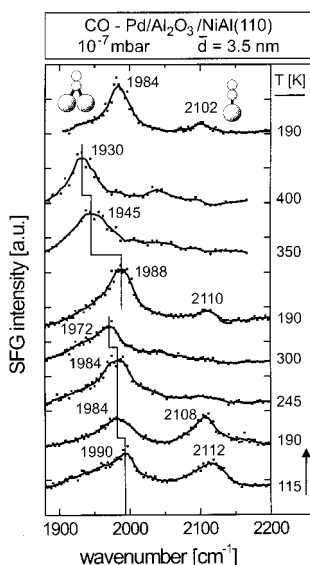


Figure 12. Effect of annealing 3.5 nm Pd nanoparticles in 10^{-7} mbar CO up to 400 K. After annealing to 300 K, a smaller fraction of on-top CO is evident from the SFG spectra.

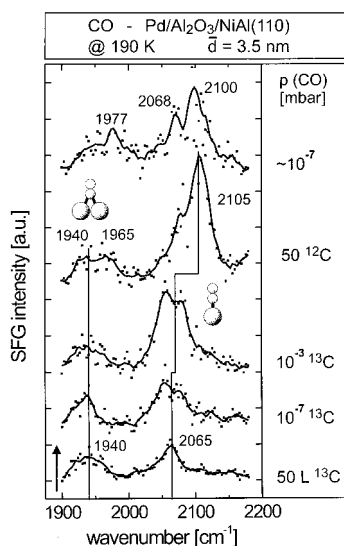


Figure 13. Isotope experiments on 3.5 nm Pd nanoparticles at 190 K illustrating the mobility of the adsorbate layer.

particles to 400 K and re-cooling to 190 K, the spectrum was not changed further.

Two reasons may account for the observed effect. The particle surface may order upon annealing to 300 K, that is, defects are healed and better-ordered facets are formed. Alternatively, cooling from 300 to 190 K in 10^{-7} mbar CO may allow formation of a better-ordered CO layer in which the stronger-bonded bridged CO dominates.^{21,25,26} However, preliminary SFG results³⁹ and IRAS data⁶⁸ suggest that the temperature-induced ordering of the Pd surface is the dominant effect (annealing of “fresh” particles to 300 K in a vacuum and recooling before CO is introduced produced changes similar to Figure 12), but more experiments will be necessary to clarify this point.

The dynamic character of the adsorbate layer is illustrated in Figure 13. Defective particles of 3.5 nm mean size were saturated with ^{13}C at 190 K. This resulted in the typical spectrum exhibiting a bridge and an on-top peak, but because of the isotope effect, the resonance frequencies were shifted to lower wavenumber (1940 and 2065 cm^{-1}), in excellent agreement with values calculated using a simple harmonic oscillator

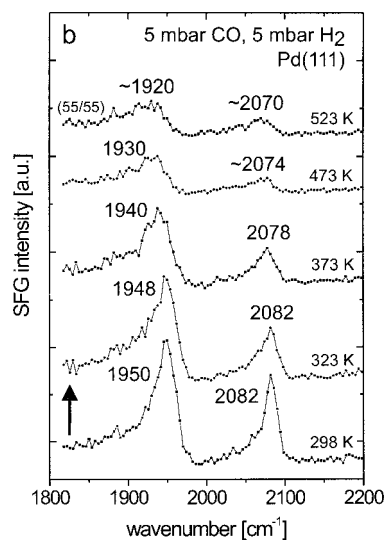
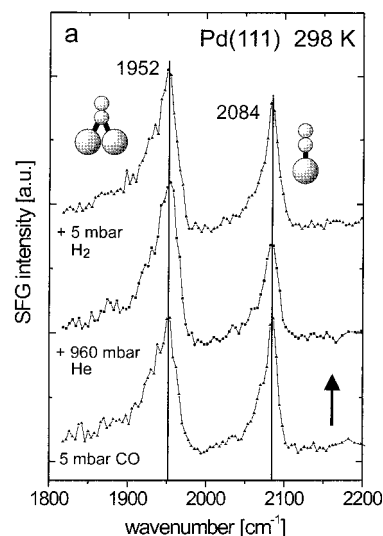


Figure 14. SFG spectra of CO and H_2 coadsorption on Pd(111): (a) sequence of gas dosing; (b) SFG spectra at increasing temperature. The CO and H_2 pressures were 5 and 5 mbar, respectively, except from the spectrum at 523 K, when 55 and 55 mbar were used.

model. Upon increasing the ^{13}C CO pressure to 10^{-7} and 10^{-3} mbar, the on-top peak increased in intensity. When the sample was exposed to 50 mbar of ^{12}C CO, the on-top peak was shifted to 2105 cm^{-1} (the resonance frequency of ^{12}C CO). Although the on-top range is dominated by ^{12}C CO, a shoulder of linear ^{13}C CO (2065 cm^{-1}) indicates that the exchange was not complete. Some strongly bound ^{13}C CO remained, presumably ^{13}C CO molecules bonded to defect or edge sites. The broad bridge peak is not shifted significantly. When the CO gas was pumped out, the spectrum exhibited peaks originating from on-top-bonded ^{12}C CO (2100 cm^{-1}) and ^{13}C CO (2068 cm^{-1}) and a broad bridge peak with a maximum around 1977 cm^{-1} (^{12}C CO). This illustrates the high mobility of the adsorbed CO molecules at 190 K.

One of the main advantages of SFG spectroscopy is that it can be carried out during a catalytic reaction, for example, during CO hydrogenation. As a first step in this direction, we have studied the coadsorption of CO and hydrogen at elevated pressure and temperature. Figure 14a shows a sequence of SFG spectra measured during dosing the “reactants”. The 5 mbar CO spectrum at 298 K shows the typical bridge and on-top peaks at 1952 and 2084 cm^{-1} . Adding 960 mbar of He makeup gas

and 5 mbar H₂ had no effect on the CO spectrum. SFG spectra were then taken at increasing temperature (Figure 14b), that is, decreasing coverage (approximately between 0.6 and 0.5 ML). The observed spectra were similar to the corresponding (pure) CO spectra, with the on-top peak desorbing first (on-top/bridge ratio at 298 and 323 K, ~0.3; at 373–523 K, ~0.2). Apparently, hydrogen had no strong influence on the adsorption site occupancy of CO because at about 0.5 ML there is sufficient space for hydrogen to adsorb and dissociate.^{69,70} However, the spectra at 473 and 523 K are somewhat different from pure CO spectra. At a coverage of 0.5 ML—when hollow CO is typically found at 1920 cm⁻¹—no linearly bonded CO should be present (Figure 2 and ref 19). The presence of on-top CO at 523 K may indicate surface roughening under reaction conditions,^{6,49,71} but this assumption awaits confirmation by further experiments.

On large Pd nanoparticles (and hence on Pd(111)), methane would be expected as the main product, while small Pd particles should produce more methanol.^{63,72} However, predictions are difficult because the selectivity is drastically influenced by the support structure (porosity) and promoters.^{63,73,74} Reaction studies utilizing higher temperatures (focusing on CH_xO intermediates^{75–77}) are in progress.

4. Conclusions

Nonlinear optical sum frequency generation (SFG) vibrational spectroscopy has been employed to study the adsorption of CO on Pd(111), “defect-rich” Pd(111), and supported Pd nanoparticles. Under UHV conditions, a surface sensitivity can be achieved that is comparable to the classical surface science methods. The spectral resolution of SFG (~5 cm⁻¹) is able to compete with IRAS, but SFG is limited by its lower signal-to-noise level. However, this optical surface science method is not restricted to solid–vacuum interfaces, and the combination of a surface analysis chamber with an SFG-compatible UHV–high-pressure cell allows the study of adsorbates on well-defined surfaces from submonolayer coverages up to ambient gas pressure.

Studies of CO adsorption on Pd(111) from 10⁻⁷ up to 1000 mbar have shown that the high-pressure adsorbate structures were comparable with saturation structures obtained at low temperature in UHV. CO adsorption on defect-rich (stepped) Pd(111) yielded an additional bridge peak that is related to surface defects. This peak could also be observed on supported Pd nanoparticles because of their surface inhomogeneity. Under UHV conditions (10⁻⁷ mbar), the CO adsorption site occupancy on Pd nanoparticles was mainly governed by the particle surface structure and temperature. For instance, at 10⁻⁷ mbar and 190 K, bridge-bonded and on-top CO coexisted on Pd particles that exhibited surface defects, while on well-faceted Pd nanocrystals CO nearly exclusively adsorbed in bridge sites. However, even for well-faceted Pd particles, on-top sites were increasingly populated at ≥ 1 mbar. The different site occupation illustrates the importance of high-pressure studies.

On Pd(111), a rearrangement of the CO layer from a bridge/on-top to a hollow/on-top configuration occurred at high coverage (between ~0.6 and 0.7 ML). In contrast, the curved surface of Pd particles presumably prevented the complete transition, even though a much higher pressure was applied (e.g., 200 mbar on particles vs 1 mbar on Pd(111) at 190 K).

At the rather low temperatures studied (300 K), no evidence for pressure-induced surface structural changes was observed. However, annealing of Pd nanoparticles to 300 K produced better-ordered surfaces and changed the SFG spectrum accord-

ingly. The dynamic character of the adsorbate layer was demonstrated by isotope experiments. Coadsorption studies of CO and H₂ on Pd(111) at elevated temperature have indicated no strong influence of hydrogen on the adsorption of CO. Combining SFG spectroscopy with a well-defined nanocluster model catalyst is certainly a promising route toward extending surface science studies to more realistic conditions.

Acknowledgment. Part of this work was supported by the Priority Program SPP 1091 of the German Science Foundation (DFG). H.U. is grateful for a DFG research fellowship. We also thank M. Heemeier and M. Bäumer (FHI Berlin) for the STM image in Figure 1c.

References and Notes

- (1) Shen, Y. R. *Surf. Sci.* **1994**, *299/300*, 551.
- (2) Richmond, G. L. *Annu. Rev. Phys. Chem.* **2001**, *52*, 357.
- (3) Hall, R. B.; Russell, J. N.; Miragliotta, J.; Rabinowitz, P. R. In *Chemistry and Physics of Solid Surfaces*; Vanselow, R., Howe, R., Eds.; Springer Series in Surface Science; Springer: Berlin, 1990; Vol. 22, p 87.
- (4) Somorjai, G. A.; McCrea, K. R. *Adv. Catal.* **2000**, *45*, 385.
- (5) Metka, U.; Schweitzer, M. G.; Volpp, H. R.; Wolfrum, J.; Warnatz, J. Z. *Phys. Chem.* **2000**, *214*, 865.
- (6) Somorjai, G. A.; Rupprechter, G. *J. Phys. Chem. B* **1999**, *103*, 1623.
- (7) Cremer, P. S.; McIntyre, B. J.; Salmeron, M.; Shen, Y. R.; Somorjai, G. A. *Catal. Lett.* **1995**, *34*, 11.
- (8) Klünker, C.; Balden, M.; Lehwald, S.; Daum, W. *Surf. Sci.* **1996**, *360*, 104.
- (9) Bandara, A.; Dobashi, S.; Kubota, J.; Onda, K.; Wada, A.; Domen, K.; Hirose, C.; Kano, S. *Surf. Sci.* **1997**, *387*, 312.
- (10) Härle, H.; Lehnert, A.; Metka, U.; Volpp, H. R.; Willms, L.; Wolfrum, J. *Chem. Phys. Lett.* **1998**, *293*, 26.
- (11) Dellwig, T.; Rupprechter, G.; Unterhalt, H.; Freund, H.-J. *Phys. Rev. Lett.* **2000**, *85*, 776.
- (12) Baldelli, S.; Eppler, A. S.; Anderson, E.; Shen, Y. R.; Somorjai, G. A. *J. Chem. Phys.* **2000**, *113*, 5432.
- (13) McIntyre, B. J.; Salmeron, M.; Somorjai, G. A. *J. Vac. Sci. Technol. A* **1993**, *11*, 1964.
- (14) Berkó, A.; Ménesi, G.; Solyósi, F. *J. Phys. Chem.* **1996**, *100*, 17732.
- (15) Rupprechter, G.; Seeber, G.; Goller, H.; Hayek, K. *J. Catal.* **1999**, *186*, 201.
- (16) Hayek, K.; Fuchs, M.; Klötzer, B.; Reichl, W.; Rupprechter, G. *Top. Catal.* **2000**, *13*, 55.
- (17) Jensen, J. A.; Rider, K. B.; Salmeron, M.; Somorjai, G. A. *Phys. Rev. Lett.* **1998**, *80*, 1228.
- (18) Freund, H.-J. *Faraday Discuss.* **1999**, *114*, 1.
- (19) Tüshaus, M.; Berndt, W.; Conrad, H.; Bradshaw, A. M.; Persson, B. *Appl. Phys. A* **1990**, *51*, 91.
- (20) Bradshaw, A. M.; Hoffmann, F. M. *Surf. Sci.* **1978**, *72*, 513.
- (21) Hoffmann, F. M. *Surf. Sci. Rep.* **1983**, *3*, 103.
- (22) Conrad, H.; Ertl, G.; Küppers, J. *Surf. Sci.* **1978**, *76*, 323.
- (23) Conrad, H.; Ertl, G.; Koch, J.; Latta, E. E. *Surf. Sci.* **1974**, *43*, 462.
- (24) Ohtani, H.; Van Hove, M. A.; Somorjai, G. A. *Surf. Sci.* **1987**, *187*, 372.
- (25) Kuhn, W. K.; Szanyi, J.; Goodman, D. W. *Surf. Sci. Lett.* **1992**, *274*, L611.
- (26) Bourguignon, B.; Carrez, S.; Dragnea, B.; Dubost, H. *Surf. Sci.* **1998**, *418*, 171.
- (27) Guo, X.; Yates, J. T. *J. Chem. Phys.* **1989**, *90*, 6761.
- (28) Surnev, S.; Sock, M.; Ramsey, M. G.; Netzer, F. P.; Wiklund, M.; Borg, M.; Andersen, J. N. *Surf. Sci.* **2000**, *470*, 171.
- (29) Szanyi, J.; Kuhn, W. K.; Goodman, D. W. *J. Vac. Sci. Technol. A* **1993**, *11*, 1969–1974.
- (30) Rainer, D. R.; Wu, M.-C.; Mahon, D. I.; Goodman, D. W. *J. Vac. Sci. Technol. A* **1996**, *14*, 1184.
- (31) Gelin, P.; Siedle, A.; Yates, J. T. *J. Phys. Chem.* **1984**, *88*, 2978.
- (32) Evans, J.; Hayden, B. E.; Lu, G. *Surf. Sci.* **1996**, *360*, 61.
- (33) Wolter, K.; Seiferth, O.; Kühlenbeck, H.; Bäumer, M.; Freund, H.-J. *Surf. Sci.* **1998**, *399*, 190.
- (34) Shen, Y. R. *Nature* **1989**, *337*, 519.
- (35) Shen, Y. R. *The Principles of Nonlinear Optics*; John Wiley Inc.: New York, 1984.
- (36) McCrea, K. R.; Somorjai, G. A. *J. Mol. Catal. A* **2000**, *163*, 43.
- (37) Caudano, Y.; Peremans, A.; Thiry, P. A.; Dumas, P.; Tadjeddine, A. *Surf. Sci.* **1996**, *368*, 337.
- (38) Williams, C. T.; Yang, Y.; Bain, C. D. *Catal. Lett.* **1999**, *61*, 7.

- (39) Unterhalt, H.; Morkel, M.; Galletto, P.; Rupprechter, G.; Freund, H.-J., to be submitted for publication, 2002.
- (40) Rupprechter, G.; Dellwig, T.; Unterhalt, H.; Freund, H.-J. *J. Phys. Chem. B* **2001**, *105*, 3797.
- (41) Rupprechter, G.; Dellwig, T.; Unterhalt, H.; Freund, H.-J. *Top. Catal.* **2001**, *15*, 19.
- (42) Bäumer, M.; Freund, H.-J. *Prog. Surf. Sci.* **1999**, *61*, 127.
- (43) Bäumer, M.; Libuda, L.; Sandell, A.; Freund, H.-J.; Graw, G.; Bertrams, T.; Neddermeyer, H. *Ber. Bunsen-Ges. Phys. Chem.* **1995**, *99*, 1381.
- (44) Hansen, K. H.; Worren, T.; Stempel, S.; Lægsgaard, E.; Bäumer, M.; Freund, H.-J.; Besenbacher, F.; Stensgaard, I. *Phys. Rev. Lett.* **1999**, *83*, 4120.
- (45) Henry, C. R. *Surf. Sci. Rep.* **1998**, *31*, 235.
- (46) Frank, M.; Bäumer, M. *Phys. Chem. Chem. Phys.* **2000**, *2*, 3723.
- (47) Shaikhutdinov, S.; Heemeier, M.; Bäumer, M.; Lear, T.; Lennon, D.; Oldman, R. J.; Jackson, S. D.; Freund, H.-J. *J. Catal.* **2001**, *200*, 330.
- (48) Nepijko, S. A.; Klimenkov, M.; Adelt, M.; Kühlenbeck, H.; Schlögl, R.; Freund, H.-J. *Langmuir* **1999**, *15*, 5309.
- (49) Rupprechter, G.; Freund, H.-J. *Top. Catal.* **2001**, *14*, 3.
- (50) Brandt, R. K.; Sorbello, R. S.; Greenler, R. G. *Surf. Sci.* **1992**, *271*, 605.
- (51) Woodruff, D. P.; Bradshaw, A. M. *Rep. Prog. Phys.* **1994**, *57*, 1029.
- (52) Greenler, R. G.; Brandt, R. K. *Colloids Surf. A* **1995**, *105*, 19.
- (53) Brandt, R. K.; Hughes, M. R.; Bourget, L. P.; Truszkowska, K.; Greenler, R. G. *Surf. Sci.* **1993**, *286*, 15.
- (54) Doyen, G.; Ertl, G. *Surf. Sci.* **1974**, *43*, 197.
- (55) Giessel, T.; Schaff, O.; Hirschmugl, C. J.; Fernandez, V.; Schindler, K. M.; Theobald, A.; Bao, S.; Lindsay, R.; Berndt, W.; Bradshaw, A. M.; Baddeley, C.; Lee, A. F.; Lambert, R. M.; Woodruff, D. P. *Surf. Sci.* **1998**, *406*, 90.
- (56) Loffreda, D.; Simon, D.; Sautet, P. *Surf. Sci.* **1999**, *425*, 68.
- (57) Härle, H.; Mendel, K.; Metka, U.; Volpp, H. R.; Willms, L.; Wolfrum, J. *Chem. Phys. Lett.* **1997**, *279*, 275.
- (58) Carrez, S.; Dragnea, B.; Zheng, W. Q.; Dubost, H.; Bourguignon, B. *Surf. Sci.* **1999**, *440*, 151.
- (59) Ortega, A.; Hoffmann, F. M.; Bradshaw, A. M. *Surf. Sci.* **1982**, *119*, 79.
- (60) Behm, R. J.; Christmann, K.; Ertl, G. *J. Chem. Phys.* **1980**, *73*, 2984.
- (61) Raval, R.; Haq, S.; Harrison, M. A.; Blyholder, G.; King, D. A. *Chem. Phys. Lett.* **1990**, *167*, 391.
- (62) Bradshaw, A. M.; Hoffmann, F. M. *Surf. Sci.* **1975**, *52*, 449.
- (63) Cabilla, G. C.; Bonivardi, A. L.; Baltanas, M. A. *Catal. Lett.* **1998**, *55*, 147.
- (64) Dellwig, T.; Hartmann, J.; Libuda, J.; Meusel, I.; Rupprechter, G.; Unterhalt, H.; Freund, H.-J. *J. Mol. Catal. A* **2000**, *162*, 51.
- (65) Rupprechter, G.; Calvino, J. J.; López-Cartes, C.; Fuchs, M.; Gatica, J. M.; Pérez-Omil, J. A.; Hayek, K.; Bernal, S. *Stud. Surf. Sci. Catal.* **2000**, *130*, 2021.
- (66) Neyman, K.; Rösch, N.; Rupprechter, G.; Libuda, J.; Freund, H.-J., to be submitted for publication, 2002.
- (67) Gusovius, A. F.; Watling, T. C.; Prins, R. *Appl. Catal. A* **1999**, *188*, 187.
- (68) Wolter, K.; Freund, H.-J. Diploma Thesis, University Bochum, Germany, 1997.
- (69) Kiskinova, M. P.; Bliznakov, G. M. *Surf. Sci.* **1982**, *123*, 61.
- (70) Hoge, D.; Tüshaus, M.; Bradshaw, A. M. *Surf. Sci.* **1988**, *207*, L935.
- (71) Kung, K. Y.; Chen, P.; Wei, F.; Shen, Y. R.; Somorjai, G. A. *Surf. Sci. Lett.* **2000**, *463*, L627.
- (72) Hicks, R. F.; Bell, A. T. *J. Catal.* **1984**, *90*, 205.
- (73) Gotti, A.; Prins, R. *J. Catal.* **1998**, *175*, 302.
- (74) Hindermann, J. P.; Hutchings, G. J.; Kiennemann, A. *Catal. Rev. – Sci. Eng.* **1993**, *35*, 1.
- (75) Sellmer, C.; Prins, R.; Kruse, N. *Catal. Lett.* **1997**, *47*, 83.
- (76) Rothaemel, M.; Zanthoff, H. W.; Baerns, M. *Catal. Lett.* **1994**, *28*, 321.
- (77) Kadinov, G.; Bonev, C.; Todorova, S.; Palazov, A.; Lietz, G.; Völter, J. *J. Mol. Catal.* **1993**, *83*, 157.